J. Fluid Mech. (1982), *vol.* 121, *pp.* 257–281
Printed in Great Britain

An extended channel model for the prediction of motion in elongated homogeneous lakes. Part 2. First-order model applied to ideal geometry: rectangular basins with flat bottom

By GABRIEL RAGGIO AND KOLUMBAN HUTTER

Laboratory of Hydraulics, Hydrology and Glaciology, The Federal Institute of Technology, Zurich, Switzerland

(Received 30 December 1980 and in revised form 28 September 1981)

A first-order channel model for fluid motion in long homogeneous lakes, as derived in detail by Raggio & Hutter (1982*a*), is presented. This model describes the motion through spatially one-dimensional boundary-value problems and is deduced by representing each field variable by cross-sectional expansions with a constant and a linear term. Various wave solutions of the governing equations applied to rectangular basins with flat bottom are presented. It is demonstrated that for moderate rotation speeds of the Earth and for elongated basins of a homogeneous fluid the main features of gravitational oscillations are predicted by the model. In particular Kelvin- and Poincaré-type waves are shown to exist. Furthermore, conditions of complete and incomplete reflections of Kelvin waves and free oscillations are discussed. The results corroborate the suitability of the model as far as wave motion in rectangular basins is concerned, but equally elucidate the physics behind them, which is less transparent when attacked with the full theory. The application of the model to basins of different shapes and to a real lake is reserved to a companion paper.

1. Introduction

Wave motions in a body of homogeneous water on the rotating Earth are characterized by a cyclonic or anticyclonic rotation of the wave vector. Several types of such waves may be distinguished. For instance, for Kelvin waves the surface elevation slope balances the effect of the Earth rotation. In the Northern hemisphere this quasi-geostrophic balance is manifested by an increase of the surface elevation to the right when looking in the direction of the wave propagation. In an enclosed basin this gives rise to waves travelling around the basin in a counterclockwise direction. In contrast to this, Poincaré-type waves appear as wave patterns rotating in either of the two directions. Standing waves do not exist, as there are no stationary nodal lines of the surface elevation. Rather, these lines rotate in the clockwise and counterclockwise directions, and thus give rise to a single stationary point, known as the amphidromic point.

Free waves in rotating systems cannot, in general, be simulated by the classical channel equation (see e.g. Chrystal 1904, 1905). These equations are purely one-dimensional, and ignore velocity and surface-elevation variations across the channel

width. At most, Kelvin waves can be obtained by superposing on this solution a surface-elevation correction from a transverse geostrophic balance (Defant 1953). This is known as the Kelvin wave-dynamics hypothesis.

For these reasons water waves in basins on the rotating Earth were analysed with two-dimensional equations – the Laplace (1829) tidal equations. Kelvin (1879) and Poincaré (1910) studied the waves mentioned above as solutions of these equations. Further, Taylor (1920) solved the reflection problem for a half-open gulf, and first discussed free oscillations in rectangular basins. Kelvin (1879) and Howard (1960) analysed solutions in polar co-ordinates. Vivid discussions with a bias towards observations are given by Mortimer (1963), and mathematical formulations for these can be found in the treatises of Lamb (1932) and LeBlond & Mysak (1978). Further, closed basins that have been treated are rectangles with constant depth (for a summary see Rao 1966), sectors with constant depth (Pnueli & Pekeris 1968), and ellipses with parabolic bottom (Ball 1965).

Guided by the appeal of the classical channel equations, Raggio & Hutter (1982*a*) derived and extended channel models in which the inconsistencies of the Chrystal equations are removed. The aim was to deduce a spatially one-dimensional set of equations from the three-dimensional equations of fluid motion in a rotating basin, which is conceptually and computationally simpler than the full three-dimensional set of differential equations and boundary conditions.

The derivation of this channel model involves the application of the weighted-residual technique in combination with a cross-sectional shape-function expansion of the field variables. The result is a hierarchy of channel models. These are applicable to a great variety of physical phenomena. Our intention here is to show that a first-order model can reasonably predict the gravitational waves mentioned above. To this end all nonlinear and friction terms in the general channel equations are omitted and shape functions are restricted to vary only in the transverse direction.

2. Scope of this study

The paper is arranged as follows. In § 3 the first-order model using a constant and linear term in the shape-function expansion (a truncated Cauchy series) is presented. This set of equations is applicable for narrow elongated natural lakes of arbitrary bathymetry. In § 4 these equations are then specialized for rectangular basins of constant depth. The emerging equations are subject to plane harmonic waves for both a non-rotating and a rotating basin. For the former, standing waves with longitudinal and antisymmetric transverse variations of surface elevation are shown to approximate the solution of the two-dimensional tidal shallow water equations. For the latter, Kelvin-type and Poincaré-type waves are deduced which nearly reproduce the corresponding wave solutions of two-dimensional equations. Superpositions of such solutions give rise to the formation of amphidromic systems. As a consequence, superposed Kelvin- and Poincaré-type waves cannot be regularly reflected at a barrier across the channel. In § 5 we therefore investigate this reflection problem. To this end a further solution is added to the above-mentioned superposed travelling-wave solutions. When this solution has boundary-layer structure, the reflection is called complete. In this case a forward-moving Kelvin-type wave will, after reflection at the barrier and far distant from the barrier, transform into a backward-moving Kelvin wave. For incomplete

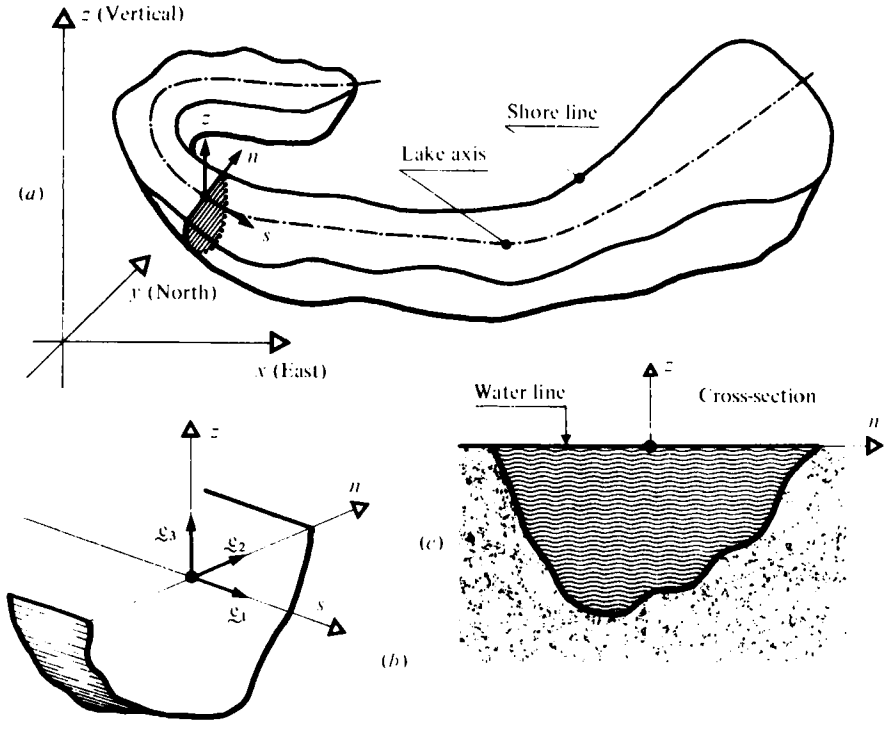

FIGURE 1. (*a*) Curved elongated basin situated in a Cartesian co-ordinate system (x, y, z) on the rotating Earth; x points towards the East, y North, and z into the vertical direction. A second co-ordinate system (s, n, z) has s measured along a prescribed lake axis, n transverse to it in the undeformed free surface, and z vertical. (*b*) Unit base vectors $\mathbf{e}_1, \mathbf{e}_2, \mathbf{e}_3$, defined along the respective 'natural' co-ordinates (s, n, z). These unit vectors are used to define the physical components of vectors. (*c*) Planes that cut the 'long' axis perpendicularly are defined as cross-sections. They are those parts of the vertical planes which are wedded by the water.

reflection this is not so, and the reflected Kelvin-type wave becomes of Poincaré type. Conditions of complete and incomplete reflection of an incident Kelvin-type wave are closely examined. This study also allows the identification of Sverdrup and inertial-type waves as exhibited by the channel equations and paves the way for the free-oscillation study in long rectangles.

Complementary results on wave motion in ring-shaped basins which further prove the suitability of the model equations are given elsewhere (Raggio 1981; Hutter & Raggio 1982), and the results on free oscillations of a model of arbitrary order applied to a natural lake are reserved for the companion paper (Raggio & Hutter 1982*b*).

3. A first-order channel model

We are concerned here with the dynamics of an incompressible inviscid fluid with free surface, occupying a slender three-dimensional domain. To describe the motion a right-handed plane orthogonal curvilinear co-ordinate system is introduced (see figure 1*a*). The domain is assumed to be long in one direction of this curvilinear co-ordinate system, and the idea is to select a line on the undisturbed lake surface as the 'axis' and to complement it with two other axes, one horizontal and the other vertical.

The selection of the long axis is arbitrary in general. Its curve parameter will be denoted by s, the co-ordinate measured horizontally by n, and that on the vertical axis by z, which is positive upwards. The co-ordinate system (s, n, z) accounts in a natural fashion for the 'bending' of the lake in its long direction, and the curvature K of the lake axis is a measure of this bending.

In Raggio & Hutter (1982*a*) a spatially one-dimensional (channel) theory was developed from the three-dimensional hydrodynamical equations. The idea was to develop each unknown field variable into a product of shape functions $\boldsymbol{\phi}$ and an equal number of parameters, so that the velocity components v_s, v_n, v_z (referred to the unit basis in figure 1*b*) and the surface elevation ξ have the representation

$$v_s = \boldsymbol{\phi} . \mathbf{v}_s, \ldots, \ldots; \quad \xi = \boldsymbol{\phi} . \boldsymbol{\xi}.$$

In general, the functions $\boldsymbol{\phi}$ depend on n and z, but for the purposes of this article the z-dependencies will be ignored so that $\boldsymbol{\phi} = \boldsymbol{\phi}(n)$. Also $\mathbf{v}_s, \ldots, \boldsymbol{\xi}$ depend on the arc length s measured along the lake axis and on time t.

A channel model is a spatially one-dimensional set of partial differential equations (and associated boundary and initial conditions) in the variables s and t for the unknowns $\boldsymbol{v}_s$, $\boldsymbol{v}_n$, $\boldsymbol{v}_z$ and $\boldsymbol{\xi}$. A linear model accounting for bottom friction and atmospheric momentum input is characterized by the equations (4.6), (4.8), (4.9) and (4.11) of Raggio & Hutter (1982*a*). These equations were subsequently specialized for *Cauchy-series expansions*. When $\boldsymbol{\phi} = \boldsymbol{\phi}(n)$, such an expansion is defined by $\boldsymbol{\phi} = (1, n, n^2, \ldots)$, and if it is first order, it is truncated at the linear terms. This unbiased two-term expansion is not the most suitable for the problems treated here, but it will be shown that with it results are excellent proving *a fortiori* the suitability of the model. Occasionally in general discussions we shall also consider other shape functions.

In the subsequent analysis the vertical velocity component v_z will not be considered, the remaining field variables are then v_s, v_n and ξ, and each of them has a two-term expansion $v_s = v_s^{(0)} + n v_s^{(1)}, \mathbf{v}_s = (v_s^{(0)}, v_s^{(1)}), \ldots$, where n is the transverse co-ordinate. There are thus six unknowns, which can be selected as components of the vector

$$\mathbf{y} = (\xi^{(0)}, v_s^{(0)}, v_n^{(0)}, \xi^{(1)}, v_s^{(1)}, v_n^{(1)}). \tag{3.1}$$

For a linear model and force-free motion the equations governing free oscillations were derived in Raggio & Hutter (1982*a*, § 5). In matrix form the equation reads

$$\mathbf{A}\mathbf{y} = \mathbf{0}, \tag{3.2}$$

where the operator $\mathbf{A}$ is given in equation (5.6) of that paper. This operator contains the coefficients C_{ij}, which are expressible as cross-sectional integrals involving as integrand functions the curvature of the lake axis, the transverse co-ordinate and/or the depth.

4. Rectangular basin

In this case curvature terms vanish, and all cross-sectional constants are independent of the longitudinal co-ordinate. Moreover, if the axis is chosen to be in the middle of the canal, and B is the width and H the depth, it is easy to show that

$$C_{m0} = BH, \quad C_{m1} = 0, \quad C_{m2} = \tfrac{1}{2}BH^3 \quad (m = 0, 1), \tag{4.1}$$

$$Z_{10} = B, \quad Z_{11} = 0, \quad Z_{12} = \tfrac{1}{2}B^3, \tag{4.2}$$

so that (3.2) becomes

$$\mathbf{By} = \mathbf{0}, \tag{4.3}$$

with

$$\mathbf{B} = \begin{array}{c} \begin{matrix} \xi^{(0)} & v_s^{(0)} & v_n^{(0)} & \xi^{(1)} & v_s^{(1)} & v_n^{(1)} \end{matrix} \\ \left[\begin{array}{cc|c|ccc|c} \frac{1}{H}g\frac{\partial}{\partial t} & g\frac{\partial}{\partial s} & 0 & 0 & 0 & 0 \\ g\frac{\partial}{\partial s} & \frac{\partial}{\partial t} & -f & 0 & 0 & 0 \\ \hline 0 & f & \frac{\partial}{\partial t} & g & 0 & 0 \\ 0 & 0 & -g & \frac{1}{12}B^2\frac{g}{H}\frac{\partial}{\partial t} & \frac{1}{12}B^2 g\frac{\partial}{\partial s} & 0 \\ 0 & 0 & 0 & \frac{1}{12}B^2 g\frac{\partial}{\partial s} & \frac{1}{12}B^2\frac{\partial}{\partial t} & -\frac{1}{12}B^2 f \\ \hline 0 & 0 & 0 & 0 & \frac{1}{12}B^2 f & \frac{1}{12}B^2\frac{\partial}{\partial t} \end{array}\right] \end{array}. \tag{4.4}$$

Physically, the first and fourth component equations in (4.3) are statements of mass balance (notice the similarity with the kinematic wave equation). The second and fifth equation stem from a longitudinal momentum balance and the remaining two equations correspond to transverse momentum balance. The system (4.3), (4.4) is particularly transparent because it makes the coupling of the motion evident. For instance, if $f = 0$, i.e. a non-rotating basin, it decouples mainly into two subsystems of which the first 2×2 upper left submatrix in (4.4) is identical with the zeroth-order Chrystal model (Raggio & Hutter 1982*a*); the second 3×3 submatrix in the middle of (4.4) extends this model to a more sophisticated lower-order model which includes the transverse pressure gradient and thus accounts adequately for transverse mass flux. For $f \neq 0$ decoupling is not possible, proving *a posteriori* that the Chrystal type of equations can only be applied rigorously for non-rotating channels. The model corresponding to the 3×3 matrix in the middle of (4.4) would be of first order in the transverse velocity. The full first-order model also includes transverse variations of v_n, and it is seen from the form of the operator $\mathbf{B}(\ )$ that this first-order transverse velocity only decouples from the lower-order model when $f = 0$.

The remainder of this section will be devoted to an analysis of the operator $\mathbf{B}(\ )$. Only the key steps of the calculations will be presented, however.

4.1. *Free oscillations in a non-rotating rectangle*

The problem we shall deal with in this section is: given a non-rotating system, $f = 0$, what are the solutions of (4.3)? Or, do the three subsystems emerging from this equation approximate the oscillating behaviour of a rectangular basin?

Standing-wave solutions to (4.3) with velocity components v_s which vanish at $s = 0$ and $s = L$ are

$$\left.\begin{aligned} \xi^{(0)} &= A_1 \cos\left(\frac{k_1\pi}{L}s\right)\cos\omega_1 t, \quad \xi^{(1)} = A_4 \cos\left(\frac{k_2\pi}{L}s\right)\cos\omega_2 t, \\ v_s^{(0)} &= A_2 \sin\left(\frac{k_1\pi}{L}s\right)\sin\omega_1 t, \quad v_s^{(1)} = A_5 \sin\left(\frac{k_2\pi}{L}s\right)\sin\omega_2 t, \\ v_n^{(0)} &= A_3 \cos\left(\frac{k_2\pi}{L}s\right)\sin\omega_2 t, \quad v_n^{(1)} = A_6 \cos\left(\frac{k_3\pi}{L}s\right)\sin\omega_3 t, \end{aligned}\right\} \tag{4.5}$$

where $k_{1,2,3}$ must have integer values. Substituting these expressions into (4.3) yields a homogeneous linear system of equations for the amplitudes $A_1, \ldots, A_6$. Its characteristic equation has the solutions

$$\left.\begin{aligned} \omega_1 &= (gH)^{\frac{1}{2}}\frac{\pi k_1}{L} = \omega_{1\text{Chrystal}}, \quad \omega_3 = 0, \\ \omega_2 &= (gH)^{\frac{1}{2}}\frac{\pi k_2}{L}\left[1 + \frac{12}{\pi^2}\left(\frac{L}{k_2 B}\right)^2\right]^{\frac{1}{2}} \simeq \omega_{2\text{Chrystal}}\left[1 + 1{\cdot}2\left(\frac{L}{k_2 B}\right)^2\right]^{\frac{1}{2}}. \end{aligned}\right\} \tag{4.6}$$

Once these are known, the amplitudes $A_1, \ldots, A_6$ can be determined; when this is done, the combined solution (4.5) has the form

$$\xi = \xi^{(0)} + n\xi^{(1)} = \left(\frac{H}{g}\right)^{\frac{1}{2}}\left\{A_2 \cos\left(\frac{k_1\pi}{L}s\right)\cos\omega_1 t + n\left[1 + \frac{12}{\pi^2}\left(\frac{L}{\kappa_2 B}\right)^2\right]^{\frac{1}{2}} A_5 \cos\left(\frac{k_2\pi}{L}s\right)\cos\omega_2 t\right\}, \tag{4.7a}$$

$$v_s = v_s^{(0)} + nv_s^{(1)} = A_2 \sin\left(\frac{k_1\pi}{L}s\right)\sin\omega_1 t + nA_5 \sin\left(\frac{k_2\pi}{L}s\right)\sin\omega_2 t, \tag{4.7b}$$

$$v_n = v_n^{(0)} + nv_n^{(1)} = -\frac{L}{\pi k_2}A_5 \cos\left(\frac{k_2\pi}{L}s\right)\sin\omega_2 t, \tag{4.7c}$$

in which k_1 and k_2 may have any integer value. Since the transverse co-ordinate n appears in a linear fashion, the model gives rise to the possibility of antisymmetric surface elevation. It must be and is indeed accompanied with transverse mass flux as seen from (4.7c). Boundary conditions at the canal shore are not matched; but this is no surprise, for the unbiased shape functions which were selected do not automatically satisfy the boundary conditions.

This problem warrants closer investigation. A clue to it is obtained by comparing the results (4.7) with those emerging from the two-dimensional tidal equations (see Krauss 1973; LeBlond & Mysak 1978) for the case $f = 0$, yielding the following. Whereas the exact solution consists of terms in which any order of sinusoidal variation of the fields in the transverse direction may occur, the solution (4.7) with the frequency

relations (4.6) only allows the lowest-order transverse mode to be taken into account. Therefore, restricting the two-dimensional solution to this mode, it is seen that the frequencies ω_1, obtained with (4.7) and the tidal equations, are identical, but that the frequencies ω_2 differ in the coefficient of the second term under the square-root sign. Denoting frequencies obtained using the two-dimensional shallow-water equations by $\omega^{(cl)}$ (for mathematical expressions see Krauss 1973; LeBlond & Mysak 1978) we may thus write

$$\frac{\omega_2}{\omega_2^{cl}} = \left[\frac{1+1{\cdot}2(L/kB)^2}{1+(L/kB)^2}\right]^{\frac{1}{2}}.$$

As far as velocities and surface elevation are concerned, a comparison of the two-dimensional solutions and formulas (4.7) reveals *that the latter are derivable from the former by a Taylor-series expansion of all functions of the transverse co-ordinate n, restricting the expanded representations to zeroth- and first-order terms.* Higher-order models using Cauchy series with more terms will improve on this Taylor-series expansion, but still violate shore boundary conditions, and shape functions which satisfy them may make the convergence in the transverse direction more uniform. This presumption is borne out very clearly if a zeroth-order model is considered having only one shape function per variable, which is the eigenfunction of the two-dimensional solution. For instance by selecting the shape functions

$$\left[\sin\left(\frac{k\pi}{B}n\right), \sin\left(\frac{k\pi}{B}n\right), \cos\left(\frac{k\pi}{B}n\right)\right] \quad \text{for} \quad (\xi, v_s, v_n) \quad (k = 1, 3, 5, \ldots),$$

$$\left[\cos\left(\frac{k\pi}{B}n\right), \cos\left(\frac{k\pi}{B}n\right), \sin\left(\frac{k\pi}{B}n\right)\right] \quad \text{for} \quad (\xi, v_s, v_n) \quad (k = 2, 4, 6, \ldots),$$

the *exact* two-dimensional solutions for the rectangular basin with flat bottom are obtained for the kth mode of transversely symmetric and skew-symmetric surface elevation respectively, and a model with an infinite number of trigonometric terms will provide the exact two-dimensional solution for all modes.

The above observations will help in the selection of more general shape functions, but it is somewhat surprising that the selection of one single shape function per variable was sufficient to model a particular mode. This is the exception, and no longer holds when $f \neq 0$, the reason being that, in rotating basins, neighbouring points move in an 'out-of-phase fashion', requiring a 'two-degrees-of-freedom description' for at least one variable. The reason for the success with the two-term Cauchy series lies in the derivation of the operator $\mathbf{B}$ given in (4.4). It is based on a weak form of the original boundary-value problem which incorporates bottom and free-surface boundary conditions (for a detailed discussion of this see Raggio & Hutter 1982*a*). Because derivation of one-dimensional models corresponds to a smoothing operation over cross-sections, errors in shore boundary conditions will also be smoothed out.

4.2. *Kelvin-type waves in an infinitely long rectangular canal*

The tidal equations permit wavelike solutions in a channel of constant cross-section for which transverse velocities v_n vanish, but whose longitudinal velocities vary exponentially in the transverse direction (see LeBlond & Mysak 1978). The operator (4.4) does not permit wavelike solutions of (4.3) with vanishing $v_n^{(0)}$ and $v_n^{(1)}$. Hence

exact reproduction of Kelvin waves is not possible with the full first-order equations, but a submodel in which longitudinal velocities and surface elevation are first order but transverse velocity is zeroth-order (this model is characterized by deleting the last column and last row in the matrix **B**) permits construction of Kelvin-type waves. Indeed by choosing

$$(\xi^{(0)}, v_s^{(0)}, v_n^{(0)}, \xi^{(1)} v_s^{(1)}) = (Z_0, U_0, V_0, Z_1, U_1) F(\kappa s - \omega t), \tag{4.8}$$

where F is any smooth function, $U_0, \ldots, Z_1$ are amplitudes, κ is the wavenumber and ω the frequency, and by substituting (4.8) into the system (4.3) (which is now reduced by one equation and one variable), one obtains

$$\left.\begin{aligned} c &= \left(\frac{\omega}{\kappa}\right)^{\frac{1}{2}} = (gH)^{\frac{1}{2}}, \\ \xi &= \xi^{(0)} + n\xi^{(1)} = \left(\frac{H}{g}\right)^{\frac{1}{2}} \left(1 \mp n\frac{f}{c}\right) U_0 F(\kappa s \mp \omega t), \\ v_s &= v_s^{(0)} + n v_s^{(1)} = \pm \left(1 \mp n\frac{f}{c}\right) U_0 F(\kappa s \mp \omega t), \\ v_n &= 0. \end{aligned}\right\} \tag{4.9}$$

Upper (lower) signs correspond to waves travelling in the positive (negative) direction of s. A progressing-wave solution has been found exhibiting Kelvin wave structure; it has the same phase speed as the two-dimensional tidal operator, and the brackets in (4.9) are truncated Taylor series of $\exp(\pm nf/c)$, arising in the exact Kelvin wave solutions. Further, adding a forward (positive-sign) and a backward (negative-sign) solution (4.9) and assuming that $F(\,) = \cos(\,)$, a Kelvin amphidromy is obtained:

$$\left.\begin{aligned} \xi &= \left(\frac{H}{g}\right)^{\frac{1}{2}} U_0 \left\{\cos \kappa s \cos \omega t - n\frac{f}{c} \sin \kappa s \sin \omega t\right\}, \\ v_s &= U_0 \left\{\sin \kappa_s \sin \omega t - n\frac{f}{c} \cos \kappa s \cos \omega t\right\}. \end{aligned}\right\} \tag{4.10}$$

Notice that there is no position $s = s_1$ for which v_s would vanish for all n and all times t. Qualitatively, this is exactly the situation encountered by Taylor (1920) when trying to solve the reflection of a Kelvin wave at the closed end of a half-open gulf. In § 4.4 a similar approach will be used.

4.3. *Wave solutions of the full first-order system – especially Poincaré-type waves*

We now return to the full system (4.3) with operator matrix (4.4) and seek travelling solutions of the form

$$\left.\begin{aligned} (\xi^{(0)}, v_s^{(0)}, \xi^{(1)}, v_s^{(1)}) &= (Z_0, U_0, Z_1, U_1) \cos(\omega t \pm \kappa s), \\ (v_n^{(0)}, v_n^{(1)}) &= (V_0, V_1) \sin(\omega t \pm \kappa s). \end{aligned}\right\} \tag{4.11}$$

Substituting (4.11) into (4.3) yields a homogeneous linear system for the unknowns $Z_0, \ldots, V_1$ which possesses non-trivial solutions if the dispersion relation

$$\sigma^6 - [\bar{\mu}^2 + 2(\gamma^2+1)]\sigma^4 + [\bar{\mu}^2(\gamma^2+1) + (\gamma^2+1)^2]\sigma^2 - \bar{\mu}^2\gamma^2 = 0 \tag{4.12}$$

is satisfied. Here

$$\left.\begin{aligned} \sigma &= \frac{\omega}{|\kappa|\,(gH)^{\frac{1}{2}}} = \frac{\omega L}{\pi(gH)^{\frac{1}{2}}}, \\ \bar{\mu}^2 &= \frac{12}{|\kappa|^2 B^2} = \frac{12}{\pi^2}\left(\frac{L}{B}\right)^2 = \frac{12}{\pi^2}\mu^2, \\ \gamma &= \frac{f}{|\kappa|\,(gH)^{\frac{1}{2}}} = \frac{fL}{\pi(gH)^{\frac{1}{2}}} \end{aligned}\right\} \tag{4.13}$$

with

$$\kappa = \pi/L, \quad \mu = L/B; \tag{4.14}$$

$1/\mu$ is the aspect ratio and σ, $\bar{\mu}$ and γ are respectively dimensionless frequency, transverse wavenumber and rotational speed all normalized with the longitudinal wavenumber κ. Two parameters thus govern the dispersion relation. The aspect ratio describes the ratio of transverse to longitudinal wavelengths. For $\mu = 1$ both are the same, and the motion has no prevailing direction. For $\mu > 1$ the elongated nature of the motion must evolve and become more and more pronounced as μ is increased. This suggests that, if our channel model is meaningful, real behaviour should be better and better approximated with increasing μ. The second parameter in the dispersion relation, γ, is a dimensionless measure of the rotation speed. According to its definition it grows with increasing f and L and with decreasing H. For homogeneous water bodies and realistic values of f, $\gamma < 1$; for reasons explained later we shall, however, also consider values of γ between 1 and 20. Once the frequency relation (4.12) is exploited, the free amplitudes $Z_0, \ldots, V_1$ can be determined; when this is done the combined solution has the form

$$\left.\begin{aligned} v_s &= v_s^{(0)} + n v_s^{(1)} = \frac{-V_0}{\omega^2 - gH\kappa^2}\left\{f\omega \pm \tau^2 \kappa g H \frac{1}{1-[f^2/\omega^2]^*}\, n\right\}\cos(\omega t \pm \kappa s), \\ v_n &= v_n^{(0)} + n v_n^{(1)} = V_0\left\{1 \mp \left[\kappa f g H \omega \frac{1}{(\omega^2 - f^2)(\omega^2 - gH\kappa^2)}\tau^2 n\right]^*\right\}\sin(\omega t \pm \kappa s), \\ \xi &= \xi^{(0)} + n\xi^{(1)} = \frac{-V_0 H}{\omega^2 - gH\kappa^2}\{\mp \kappa f - \tau^2 \omega n\}\cos(\omega t \pm \kappa s), \end{aligned}\right\} \tag{4.15}$$

where for reasons of further comparison the abbreviation

$$\tau^2 = \frac{\omega^2 - f^2 - gH\kappa^2}{gH} \tag{4.16}$$

has been used. This solution may be contrasted with the Poincaré (1910) solutions of the tidal operator. There are two classes having dispersion relation (4.21*a*) below (see Krauss 1973; LeBlond & Mysak 1978). In the limit as $f \to 0$ one class has transversely antisymmetric, and the other symmetric, surface elevation. When expanding these solutions into Taylor series of n and truncating at the lowest-order terms, the 'antisymmetric' solution reveals (4.15) except for the terms indicated by [ ]*. But these turn out to be small when exploiting the frequency relation for practical values of the rotation speed, and hence can be ignored. The 'symmetric' solution is not approximated by (4.15), but this is no surprise, for in the limit $f \to 0$, ξ in (4.15) is odd in the transverse co-ordinate.

On the other hand it is not difficult to see that by replacing the simple powers of the Cauchy-series expansions by trigonometric functions (cosine for 'symmetric' and

sine functions for 'skew-symmetric' elevations) better solutions of either types of Poincaré waves could have been found.

There remains the proof that the approximate dispersion relation (4.12), which has three real roots, gives accurate values for the frequency–wavenumber relationship for all waves characterizing rotating systems. Moreover, since energy propagates with the group velocity, sufficient agreement of the latter in the two formulations should also be obtained.

Since the dispersion relation may be written as $f(\omega, \kappa) = 0$ one has

$$\frac{\partial f}{\partial \omega} d\omega + \frac{\partial f}{\partial \kappa} d\kappa = 0, \tag{4.17}$$

and hence

$$c_{\mathrm{gr}} = \frac{d\omega}{d\kappa} = -\frac{\partial f/\partial \kappa}{\partial f/\partial \omega}. \tag{4.18}$$

Following this rule, using (4.12) it is not difficult to show that

$$\frac{c_{\mathrm{gr}}}{(gH)^{\frac{1}{2}}} = \frac{1}{\sigma} \alpha_{\mathrm{gr}}, \tag{4.19}$$

with

$$\alpha_{\mathrm{gr}} = \frac{\sigma^2\{2\sigma^2 - (\bar{\mu}^2 + 2(1+\gamma^2))\} + \bar{\mu}^2\gamma^2}{\sigma^2\{3\sigma^2 - 2(\bar{\mu}^2 + 2(1+\gamma^2))\} + \bar{\mu}^2(1+\gamma^2) + 1}. \tag{4.20}$$

This must be compared with the group velocity of the classical theory, for which the dispersion relations read

$$\sigma_{\mathrm{cl}}^2 - \mu^2 - \gamma^2 - 1 = 0, \quad \text{Poincaré-type waves,} \tag{4.21a}$$

$$\sigma_{\mathrm{cl}}^2 - 1 = 0, \quad \text{Kelvin-type waves,} \tag{4.21b}$$

$$\sigma_{\mathrm{cl}}^2 - \mu^2 - \gamma^2 = 0, \quad \text{Sverdrup-type waves,} \tag{4.21c}$$

$$\sigma_{\mathrm{cl}}^2 - \gamma^2 = 0, \quad \text{inertial-type waves,} \tag{4.21d}$$

where σ_{cl} denotes the frequency of the classical theory.

These yield for group velocity of the classical theory $c_{\mathrm{gr}}^{(\mathrm{cl})}$

$$\frac{c_{\mathrm{gr}}^{(\mathrm{cl})}}{(gH)^{\frac{1}{2}}} = \begin{cases} \sigma^{-1}, & \text{for Poincaré-, Kelvin-, Sverdrup-type waves,} \\ 0, & \text{for inertial-type waves.} \end{cases} \tag{4.22}$$

Therefore, if the approximate formulation models energy propagation properly, the factor α_{gr} should be close to unity or zero, respectively, depending on which of the above wave types is considered.

The dispersion relation (4.12) and the group-velocity formula (4.20) have been analysed numerically. In view of the discussion following (4.14) the dimensionless frequency σ should be plotted as a function of the aspect ratio, firstly when γ is held fixed, and secondly when μ is held constant but γ is varied. This will give information regarding the significance of both the rotation of the basin and the elongated nature of the motion. An example of this study is shown in figure 2. For $\gamma = 0{\cdot}5$ the three real roots of (4.12) are displayed as functions of μ in figure 2 (a). Solid lines will henceforth correspond to solutions of (4.12); dashed lines indicate the exact frequency relations as

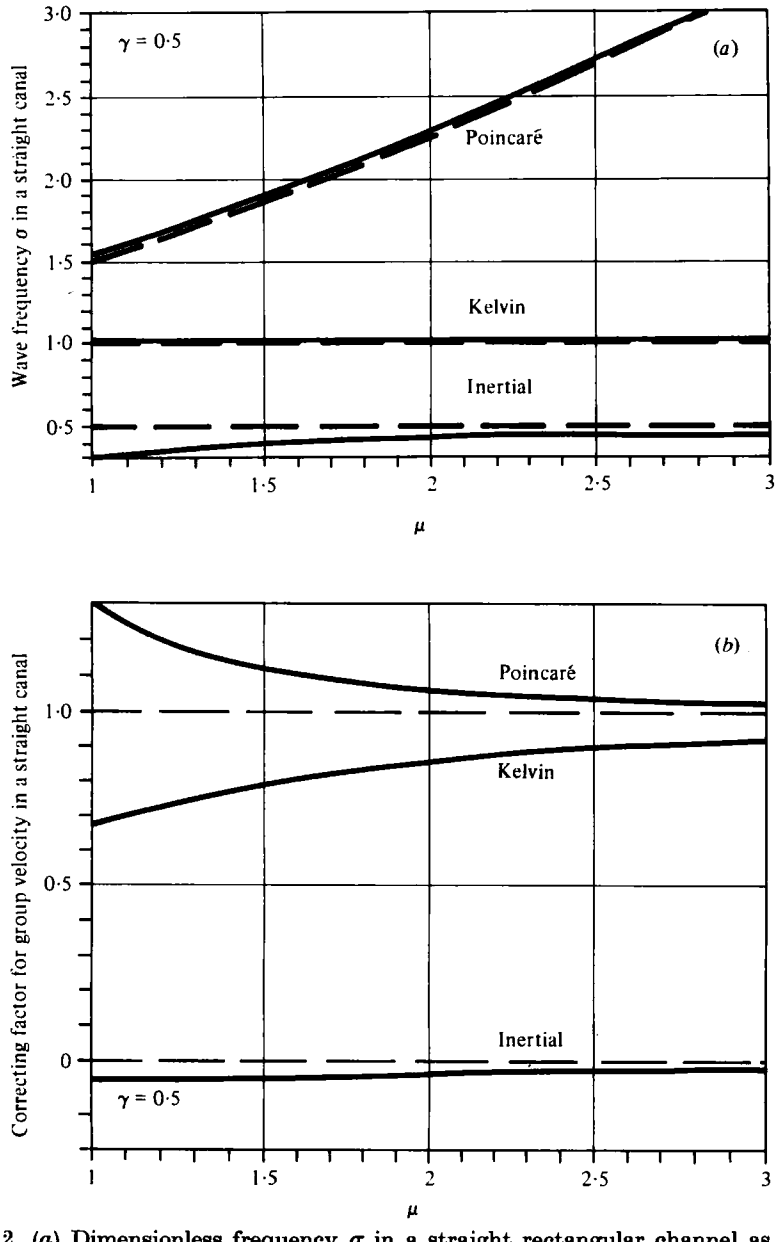

FIGURE 2. (*a*) Dimensionless frequency σ in a straight rectangular channel as obtained from (4.12), plotted against $\mu = L/B$, for $\gamma = f/\kappa(gH)^{\frac{1}{2}} = 0{\cdot}5$. Dashed lines are for the dispersion relation of the exact two-dimensional tidal operator. (*b*) Dimensionless correction factor α_{gr} in a straight rectangular channel plotted against μ for $\gamma = 0{\cdot}5$. Dashed lines correspond to exact results.

shown in (4.21). The three different solutions can be interpreted respectively as a Poincaré-type, a Kelvin-type and an inertial-type wave. To explain these interpretations notice that the Poincaré-type frequency σ approaches μ as μ becomes large, which resembles the tendency exhibited by the classical Poincaré waves. The second solution $\sigma \simeq 1$ represents the Kelvin-type frequency. By inspection, (4.15) show that

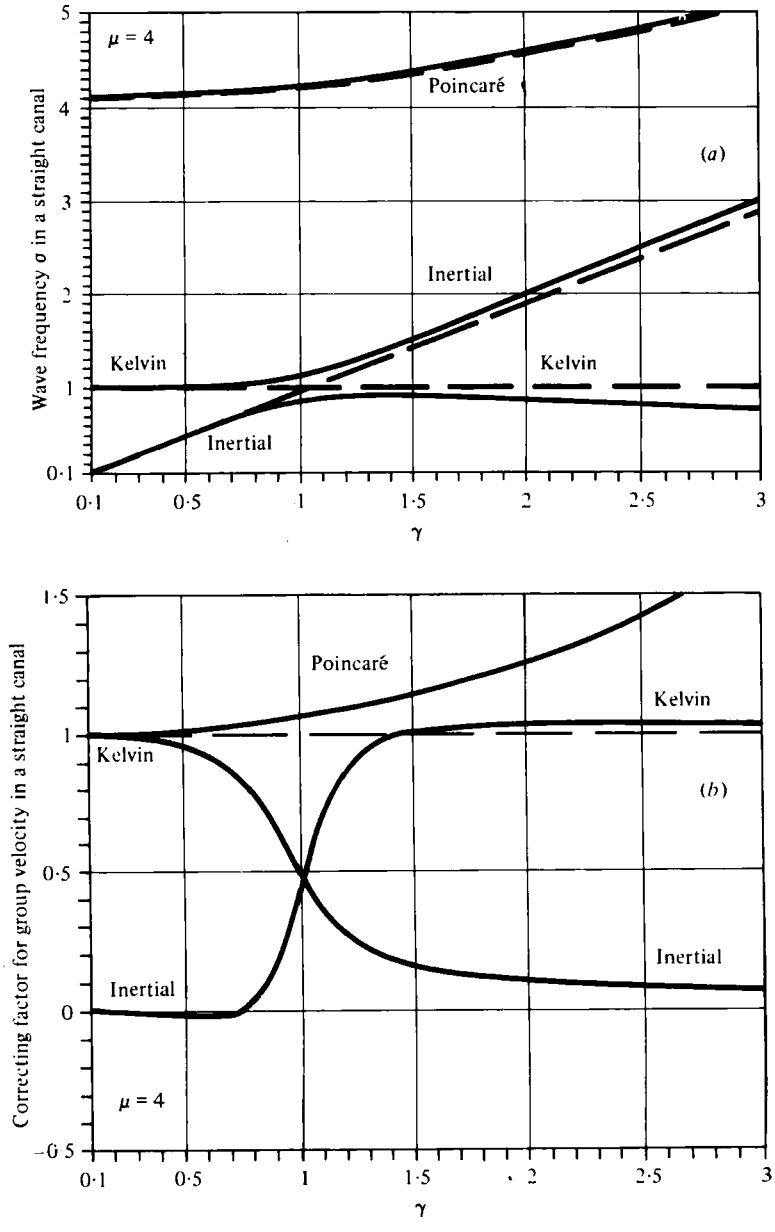

FIGURE 3. (*a*) Dimensionless frequency σ in a straight rectangular channel as obtained from (4.1), plotted against $\gamma = f/\kappa(gH)^{\frac{1}{2}}$ for $\mu = 4$. Solid lines are those of the channel model, dashed lines correspond to the exact tidal operator. (*b*) Dimensionless correcting factor α_{gr} for the group velocity in a straight rectangular channel plotted against $\gamma = f/\kappa(gH)^{\frac{1}{2}}$ for $\mu = 4$. The dashed lines at $\alpha_{gr} = 1, 0$ correspond to the respective values of the two-dimensional tidal operator.

in this case the amplitude of v_n is small compared with that of v_s. To see this, replace the free amplitude V_0 in (4.15) by $\overline{V}_0(\omega^2 - gH\kappa^2)$, where $\overline{V}_0$ is now arbitrary, and observe that for Kelvin waves $\omega^2 \simeq gH\kappa^2$. This guarantees for $\overline{V}_0$ of order unity that V_0 and therefore v_n are small, while the amplitude of v_s becomes of order unity. This same procedure also shows that the amplitude of ξ is bounded away from zero. This is

approximately tantamount to a classical Kelvin wave. The third solution resembles an inertial-type motion, for σ approaches γ as μ increases. Exploring (4.15) for frequencies ω near f also indicates that the absolute value of ξ remains small, while those for v_n and v_s are large (compare for example the terms indicated by [ ]*). This corresponds to inertial motion in which vertical displacements are very small, although horizontal velocities may have appreciable values.

To demonstrate the accuracy of the model as far as group velocities are concerned, we have displayed in figure 2(*b*) the group-velocity correction factor α_{gr} defined in (4.22) as a function of μ for the three waves and for $\gamma = 0{\cdot}5$. The results of the exact theory are shown dashed. For Poincaré- and Kelvin-type waves the value of this factor is indeed close to 1, *provided that* μ *is not too close to* 1. $\mu = 1$ corresponds to a wave that has the same wavelength in the longitudinal and transverse directions, whereas our channel equations were deduced for elongated basins and are thus applicable to motions with dominant longitudinal components, thus group velocities can hardly be reasonably well predicted, when μ is close to unity. For the third wave type, energy propagates very slowly, since $\alpha_{gr} \simeq 0$. This corresponds to inertial-type waves.

Having indicated that the approximate model is reasonable for a small value of the rotation speed γ and for all aspect ratios such that $\mu \geqslant 2$, roughly, it is interesting to see how the approximate dispersion relation (4.12) compares with the exact counterpart (4.21) when μ is held fixed and the rotation speed γ is varied. This is shown in figure 3, in which the dispersion relations (4.12) and (4.21) are graphically displayed for $0 < \gamma < 3$ and $\mu = 4$. Figure 3(*a*) shows the dimensionless frequency σ plotted against γ. Evidently, Poincaré-type, Kelvin-type and inertial-type wave solutions can be differentiated. Figure 3(*a*) indicates further that, qualitatively, exact and approximate frequency curves are close (errors will be quantified below). The structure of the frequency curves for Kelvin- and inertial-type waves near $\gamma = 1$ is of some interest. As γ increases, a Kelvin-type wave at small values of γ becomes an inertial-type wave at large values of γ, and vice versa. The frequency curves of the approximate dispersion relation do not cross but only nearly touch each other. This will be called a 'kissing mode'. We have found it to be the location where the corresponding group velocities are poorly predicted (figure 3*b*). Further reasons for the existence of this transition zone can be found in § 5 and figure 7.

In figure 3(*b*) we have also plotted the group-velocity correcting factor α_{gr} for the same three waves, dashed lines indicating the corresponding values for the exact theory. Group velocities for Poincaré waves are only predicted accurately for rotation speeds $\gamma < 1$, approximately, and those for Kelvin-type and inertial-type waves are poor when $\gamma \simeq 1$. This is exactly the region of the 'kissing mode' in figure 3(*a*). The results of figure 3(*a*) indicate that for the given value of μ and the range of values for γ Poincaré-type waves appear to be reasonably well predicted. This is borne out very clearly in figure 4(*a*, *b*) which show plots of the dimensionless Poincaré frequency as a function of γ and μ, respectively. Calculations were performed for

$$0 < \gamma < 20, \quad 1 < \mu < 20.$$

$\gamma = 0$ means no rotation or an infinitely deep basin, $\gamma = 20$ is an upper bound when a two-layer model like that of Csanady (1972) is considered, in which a reduced gravity constant and a reduced depth are introduced to calculate thermocline displacements. For homogeneous lakes γ is certainly less than 1.

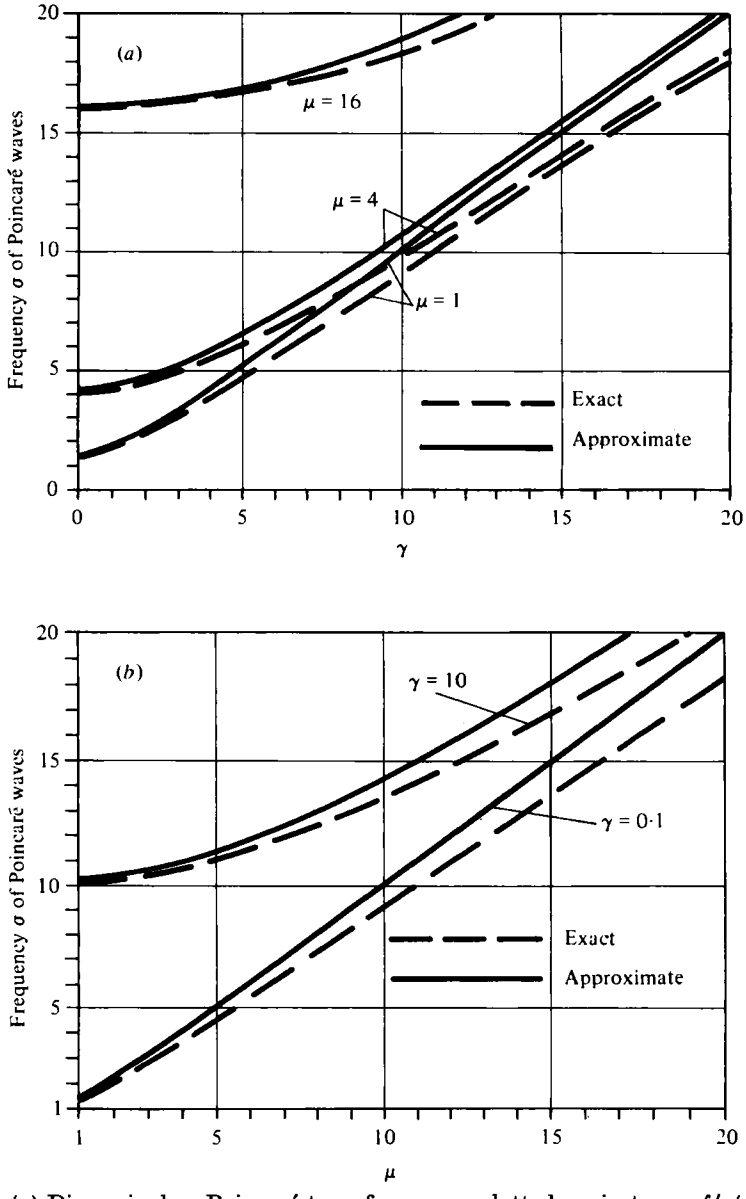

FIGURE 4. (*a*) Dimensionless Poincaré-type frequency plotted against $\gamma = f/\kappa(gH)^{\frac{1}{2}}$ for various values of $\mu = L/B$. Solid lines correspond to the channel model, dashed lines are for the two-dimensional tidal operator. (*b*) Dimensionless frequency σ of the Poincaré-type waves plotted against μ for various values of γ. Solid lines are for the channel model, dashed lines for the two-dimensional tidal operator.

The discrepancies between exact and approximate frequencies grow with increasing γ, yet relative errors $|(\sigma - \sigma_{\mathrm{cl}})/\sigma_{\mathrm{cl}}|$ stay below 10^{-1}, and are extremely small when $\gamma < 1$. Frequencies and therefore phase speeds for Poincaré waves being well predicted does not imply that group velocities for these waves are also obtained accurately. Exact and approximate dimensionless group velocities are given by (4.22) and (4.19) respectively, in which σ must obey the dispersion relations (4.21) and (4.12) respec-

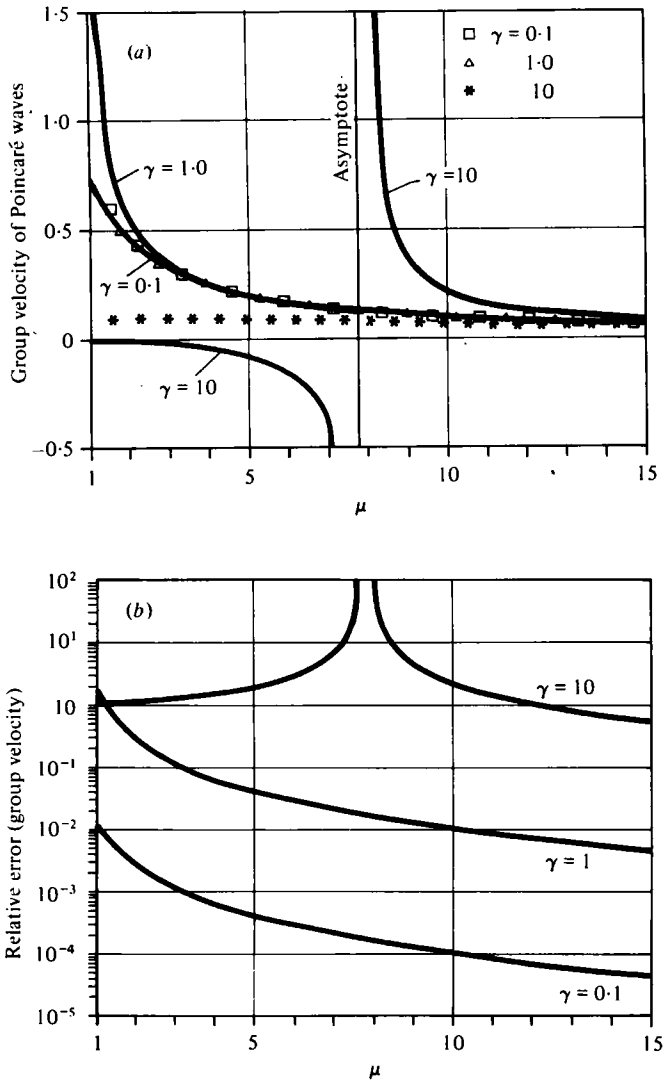

FIGURE 5. (*a*) Dimensionless group velocity of Poincaré-type waves for the two-dimensional theory and the channel model, plotted against μ for γ = (0·1, 1, 10). Solid lines correspond to results of the channel model, symbols indicate group velocities of two-dimensional tidal operator. (*b*) Relative error of the group velocity of Poincaré-type waves when calculated according to the classical and approximate models respectively.

tively. Results are displayed in figure 5(*a*), where solid lines correspond to the dimensionless group velocity of the approximate model and symbols stand for that of the exact theory. For $\gamma \leqslant 1$ agreement is fair unless μ is about unity and slightly larger and relative errors $|c_{\mathrm{gr}}^{(\mathrm{cl})} - c_{\mathrm{gr}}|/|c_{\mathrm{gr}}^{(\mathrm{cl})}|$ are small (figure 5*b*). On the other hand, for $\gamma = 10$ the approximate group velocity has a pole approximately at $\mu = 8$. The location of this pole is obtained from (4.20) by setting $\alpha_{\mathrm{gr}} = \infty$. In the classical (exact) formulation it does not arise, implying that large relative errors must evolve from the application of the channel model in the neighbourhood of these points. This is corroborated in figure 5(*b*).

The above considerations, together with further scrutiny of the dispersion relation of the full first-order model operating in rectangular basins (equation (4.4)), indicates that the extended channel theory for the tidal operator based on a two-term Cauchy-series expansion predicts frequency–wavenumber relationships accurately enough, provided that (i) the longitudinal wavelength is about twice as large (or larger) than the width of the channel, (ii) rotational speeds γ (defined in (4.13)) stay below unity. This indicates that the model should *not* be used for a two-layer model with reduced height and density as proposed by Csanady (1972). In such a model rotation speeds are larger than unity, and group velocities and hence energy-propagation speeds are incorrectly predicted, as we have just seen above.

On the other hand, calculations with higher-order models indicate that these poles might be removed to locations outside the practical ranges of the parameters. However, an insufficient number of calculations have been performed to make this statement firmly.

5. Reflection of Kelvin-type waves at a barrier of a half-open rectangular canal and free oscillations in rectangles

In order to find the complete reflection for Kelvin-type waves (see Taylor 1920) we seek wave solutions that allow for exponential decay of the fields involved as one moves away from the barrier. We thus assume

$$\left.\begin{aligned}(\xi^{(0)}, v_n^{(0)}, v_s^{(1)}) &= (Z_0, C_1, B_1)\, e^{-\lambda s}\cos\omega t,\\ (v_s^{(0)}, \xi^{(1)}, v_n^{(1)}) &= (A_1, Z_1, D_1)\, e^{-\lambda s}\sin\omega t,\end{aligned}\right\} \tag{5.1}$$

in which λ may be complex. Depending on the sign of $\mathscr{R}(\lambda)$, these fields decay exponentially as one moves into the positive or negative s-direction. Substituting (5.1) into (4.3) yields a homogeneous linear system of equations for the amplitudes, whose characteristic equation agrees with (4.12) and (4.13) if the substitution $\lambda = +i\kappa$ is made. For values of λ satisfying this equation the combined solution (5.1), found as in (4.7), has the form

$$v_s = A_1 e^{-\lambda s}\left\{\sin\omega t + n\lambda\omega\,\frac{\lambda^2 gH+\omega^2-f^2}{f(f^2-\omega^2)}\cos\omega t\right\}, \tag{5.2a}$$

$$v_n = A_1 e^{-\lambda s}\left\{\frac{\lambda^2 gH+\omega^2}{gf}\cos\omega t - n\lambda\,\frac{\lambda^2 gH+\omega^2-f^2}{f^2-\omega^2}\sin\omega t\right\}, \tag{5.2b}$$

$$\xi = A_1 e^{-\lambda s}\left\{-\frac{\lambda H}{\omega}\cos\omega t + n\,\frac{\lambda^2 gH+\omega^2-f^2}{gf}\sin\omega t\right\}, \tag{5.2c}$$

where A_1 is a constant. To explore the dispersion relation for conditions that assign to (5.2) a boundary-layer structure, we recall that adding a forward- and backward-moving Kelvin-wave solution (4.9) has not led to a valid solution for a closed channel (see (4.10)) since there is no position $s = s_1$ with no motion for all n and all t. The same inferences can be drawn for (4.15), which would lead to both Poincaré-type and Kelvin-type amphidromies. However, on adding (4.10) (or (4.15)) to (5.2), positions of no motion can be found; we shall demonstrate this with the simpler Kelvin solution

(4.10). Conditions of reflection at a barrier $s = s_1$ are $v_s(s_1) = 0$, or with an obvious notation

$$v_s^{\text{Kelvin}}(s_1) + v_s^{\text{exp}}(s_1) = 0, \tag{5.3}$$

which must hold for all time. Substitution from (4.10) and (5.2) into (5.3) yields

$$A_1 = -U_0 e^{\lambda s_1} \sin \kappa s_1 \tag{5.4}$$

$$\tan \kappa s_1 = -\frac{\exp(-\lambda s_1)}{(gH)^{\frac{1}{2}} \lambda \omega \dfrac{\lambda^2 gH + \omega^2 - f^2}{f^2(f^2 - \omega^2)}}. \tag{5.5}$$

Reflection of a Kelvin wave of given frequency ω and given wavenumber κ at a barrier located at $s = s_1$ thus affords evaluation of λ and s_1 from (4.12) (κ is replaced by $-i\lambda$) and (5.5). Equation (5.4) then yields A_1 in terms of the remaining quantities, and the compound wave is obtained when (4.10) and (5.2) are added. With $c^2 = gH$,

$$v_s = U_0 \Big\{ [\sin \kappa s - \exp(-\lambda(s - s_1)) \sin \kappa s_1] \sin \omega t - n \left[\frac{f}{c} \cos \kappa s + \exp(-\lambda(s - s_1)) \sin \kappa s \, \omega \frac{\lambda^2 c^2 + \omega^2 - f^2}{f(f^2 - \omega^2)} \right] \cos \omega t \Big\}, \tag{5.6a}$$

$$v_n = U_0 \exp(-\lambda(s - s_1)) \sin \kappa s_1 \left\{ \frac{\lambda^2 c^2 + \omega^2}{gf} \cos \omega t - n\lambda \frac{\lambda^2 c^2 + \omega^2 - f^2}{f^2 - \omega^2} \sin \omega t \right\}, \tag{5.6b}$$

$$\xi = U \left(\frac{H}{g} \right)^{\frac{1}{2}} \Big\{ \left[\cos \kappa s - \exp(-\lambda(s - s_1)) \frac{\lambda c}{\omega} \sin \kappa s_1 \right] \sin \omega t - n \left[\frac{f}{c} \sin \kappa s + \exp(-\lambda(s - s_1)) \frac{\lambda^2 c^2 + \omega^2 - f^2}{fc} \sin \kappa s_1 \right] \sin \omega t \Big\}. \tag{5.6c}$$

As is evident, a Kelvin wave propagating along one side of a half-open rectangular basin cannot always be regularly reflected as a *proper* Kelvin wave (propagating along the other side and in the opposite direction), because far distant from the barrier as $s \to \pm \infty$ the exponential solution has true exponential behaviour only when $\mathscr{R}(\lambda) \gtrless 0$, for which this contribution is asymptotically small. This corresponds to Taylor's (1920) problem, but our approximate analysis is very much simpler than was his. Frequency ranges for which the exponential decay in (5.6) occurs lead to solutions with boundary-layer structure and the reflection is *complete*. If λ is imaginary there is no exponential decay, and a forward-moving Kelvin wave cannot be reflected as a backward-moving Kelvin wave – an *incomplete* reflection.

To determine the frequency ranges where solutions with boundary-layer character may exist, we renormalize the quantities (4.13) and (4.14) with $\bar{\mu}$, and introduce

$$\bar{\sigma} = \frac{\sigma}{\bar{\mu}} = \frac{\omega B}{(12gH)^{\frac{1}{2}}}, \quad \bar{\kappa}^2 = \frac{1}{\bar{\mu}^2} = \tfrac{1}{12}\pi^2 \left(\frac{B}{L} \right)^2 = \frac{\kappa^2}{(12/B)^2} = -\frac{\lambda^2}{(12/B)^2}, \quad \bar{\gamma} = \frac{\gamma}{\bar{\mu}} = \frac{fB}{(12gH)^{\frac{1}{2}}}. \tag{5.7a,b,c}$$

The dimensionless frequency $\bar{\sigma}$ is a parameter which involves the essential quantities characterizing the reflection, namely the width B (instead of the longitudinal wavelength L, which has less physical relevance since the channel is semi-infinite), the depth

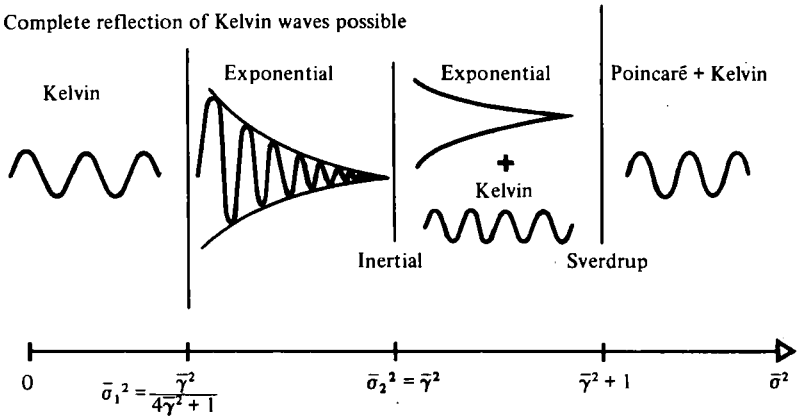

FIGURE 6. Wavenumber $\bar{\kappa}$ in the frequency range and for the two-dimensional dispersion relation.

H of the channel, and the frequency ω of the wave. The characteristic equation (4.12) may then be written as

$$Ax^2+Ex+C=0, \tag{5.8}$$

where

$$x=\bar{\kappa}^2, \tag{5.9}$$

$$A=\bar{\sigma}^2, \quad E=(2\bar{\sigma}^2-1)(\bar{\gamma}^2-\bar{\sigma}^2), \quad C=\bar{\sigma}^2(\bar{\sigma}^2(\bar{\sigma}^2-1-2\bar{\gamma}^2)+\bar{\gamma}^2(1+\bar{\gamma}^2)). \tag{5.10}$$

For a given frequency $\bar{\sigma}$ and given rotation speed $\bar{\gamma}$, $\bar{\kappa}$ is determined from (5.8), which alternatively gives λ, and boundary-layer solutions emerge when $\bar{\kappa}$ has imaginary parts. To decide this it suffices to analyse the discriminant D of the parabola (5.8). For, if $D \gtreqless 0$, there are two real roots, a real double root and two conjugate complex roots, respectively. As a function of $\bar{\sigma}^2$ the discriminent D describes the parabola,

$$D=(4\bar{\gamma}^2+1)\bar{\sigma}^4-2\bar{\gamma}^2(2\bar{\gamma}^2+1)\bar{\sigma}^2+\bar{\gamma}^4. \tag{5.11}$$

The positive roots of $D=0$ are

$$\bar{\sigma}_1=\frac{\bar{\gamma}}{(4\bar{\gamma}^2+1)^{\frac{1}{2}}}, \quad \bar{\sigma}_2=\bar{\gamma}, \tag{5.12}$$

negative roots need not be evaluated since they correspond to the same oscillation. So, for positive σ

$$D\begin{cases} >0 & (\bar{\sigma}<\bar{\sigma}_1, \quad \bar{\sigma}>\bar{\sigma}_2), \\ =0 & (\bar{\sigma}=\bar{\sigma}_1, \quad \bar{\sigma}=\bar{\sigma}_2), \\ <0 & (\bar{\sigma}_1<\bar{\sigma}<\bar{\sigma}_2). \end{cases} \tag{5.13}$$

For $\bar{\sigma}_1<\bar{\sigma}<\bar{\sigma}_2$ the characteristic equation (5.8) possesses four complex roots $\bar{\kappa}_{1,2,3,4}$, and thus the resulting solutions (5.2) viewed as functions of position have oscillatory exponential character as one moves away from the barrier. This is indicated in figure 6; it corresponds to complete reflection.

Consider next the two isolated points on the frequency axis where the discriminant D vanishes. For $\bar{\sigma}=\bar{\sigma}_2=\bar{\gamma}$, $\bar{\kappa}_{1,2,3,4}=0$, and no wave propagates along the s-axis.

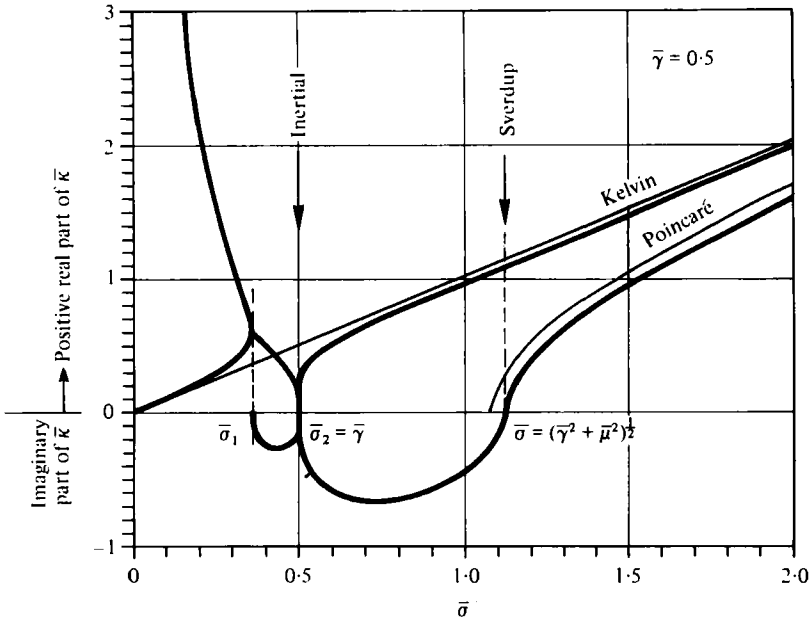

FIGURE 7. Wavenumber $\bar{\kappa}$ in the frequency range. Either two real (of a total of four) roots or a positive real and a negative imaginary part of the four complex roots are plotted. Thick lines correspond to the channel approximation, thin lines to the two-dimensional tidal operator. Inertial and Sverdrup wave motions are well predicted by the model, as is the superinertial branch $\bar{\sigma} > \bar{\gamma}$.

Scrutiny of (4.15) shows that surface elevations ξ are very small while velocities are not. The corresponding motion is therefore of inertial type. For $\bar{\sigma} = \bar{\sigma}_1$ (5.8) possesses only real solutions for the $\bar{\kappa}$s, and thus the waves are purely oscillatory.

The above relates to the interval $\bar{\sigma}_1 \leqslant \bar{\sigma} \leqslant \bar{\sigma}_2$ as shown in figure 6. Three different wave types have already been encountered. For $\bar{\sigma} = \bar{\sigma}_1$, incomplete reflection arises; when $\bar{\sigma}_1 < \bar{\sigma} < \bar{\sigma}_2$, complete reflection is possible and when $\bar{\sigma} = \bar{\sigma}_2 = \bar{\gamma}$ no wave propagates. It is advantageous to interrupt the discussion here and to complement figure 6 with figure 7. It shows for given frequency $\bar{\sigma}$ in the range $0 < \bar{\sigma} < 2$ and for given rotation speed $\bar{\gamma} = 0{\cdot}5$ real and imaginary parts of $\bar{\kappa}$ as obtained by exploiting both the frequency relation (5.8) of the channel approximation and the corresponding exact frequency relations (4.21) (written in terms of the overbarred quantities). Because we are only interested in the reflection properties of (5.6), and since $\bar{\kappa}$ and λ are related by (5.7*b*), it suffices to plot either two real parts of $\bar{\kappa}$ (of all four real roots) or else when the $\bar{\kappa}$s are complex one positive real part and one negative imaginary part. This is done in figure 7. A real $\bar{\kappa}$ (imaginary λ) will correspond to a purely oscillatory solution, and a conjugate complex $\bar{\kappa}$ will give rise to exponentially decaying (positive imaginary part) oscillatory behaviour. The classical Kelvin- and Poincaré-type waves, obtained from (4.21) and (5.7), are plotted as thin lines and inertial- and Sverdrup-type waves are marked as the points for which $\bar{\kappa} = 0$, $\bar{\sigma} = \bar{\gamma}$ and $\bar{\sigma} = (\bar{\mu}^2 + \bar{\gamma}^2)^{\frac{1}{2}}$. Thick solid lines correspond to the channel solution using the two-term Cauchy-series expansion. It is seen that in the subinertial range $\sigma_1 \leqslant \bar{\sigma} < \bar{\gamma}$ the exact theory and the channel model lie far apart. This is a first indication that

difficulties might arise with the channel approximation for wave motions at sub-inertial frequencies.

It still remains to discuss the case for which $D > 0$ in (5.11). According to the lemma of Vieta applied to the parabola (5.8) one has

$$x_1 + x_2 = \frac{(2\bar{\sigma}^2 - 1)(\bar{\sigma}^2 - \bar{\gamma}^2)}{\bar{\sigma}^2}, \tag{5.14}$$

$$x_1 x_2 = \bar{\sigma}^2(\bar{\sigma}^2 - 1 - 2\bar{\gamma}^2) + \bar{\gamma}^2(1 + \bar{\gamma}^2), \tag{5.15}$$

where x_1 and x_2 are the two roots of (5.8). Some cases have to be distinguished. For $\bar{\sigma} < \bar{\sigma}_1$ the right-hand sides of (5.14) and (5.15) are positive, so all $\bar{\kappa}$s assume real values and all waves with frequencies $\bar{\sigma}^2 \leqslant \bar{\gamma}^2/(4\bar{\gamma}^2 + 1) = \bar{\sigma}_1^2$ are purely oscillatory. Two of these waves can be interpreted to have Kelvin character, the other two are due to the mathematical approximation of the channel model and have no physical interpretation. This follows from figure 7, which shows that two wavenumbers are close to those of the classical Kelvin waves, but it can also be inferred from a careful analysis of the velocities and surface elevations (5.2), that correspond to these solutions.

The superinertial domain $\bar{\sigma} > \bar{\sigma}_2 = \bar{\gamma}$ separates into two subdomains as follows. For $\bar{\sigma}^2 = \bar{\mu}^2 + \bar{\gamma}^2, x_1 + x_2 > 0, x_1 x_2 = 0$. Thus there are two solutions where the $\bar{\kappa}$s are positive, representing two oscillatory solutions and two solutions where no wave propagates in the direction of the channel axis, since the $\bar{\kappa}$s vanish. The first is of Kelvin type. The latter represents Sverdrup waves. For $\bar{\sigma}^2 > \bar{\mu}^2 + \bar{\gamma}^2$ the right-hand sides of (5.14) and (5.15) are positive, and the emerging waves are thus oscillatory. These waves are of Poincaré and Kelvin type and have no boundary-layer structure (see figure 6). As is evident from figure 7, the classical solutions and the approximations are close.

Finally, for $\bar{\sigma}_2^2 < \bar{\sigma}^2 < \bar{\mu}^2 + \bar{\gamma}^2$, since $x_1 x_2 < 0$, but $x_1 + x_2 > 0$, two $\bar{\kappa}$s are real and two are imaginary, giving rise to exponential and/or purely oscillatory solutions with Kelvin behaviour (figures 6 and 7). The latter figure clearly shows where Kelvin- and Poincaré-type waves are reasonably predicted by the channel model. The shift between the exact Poincaré solution and that of the channel model is due to the use of Cauchy expansions. Also the superinertial ($\bar{\sigma} > \bar{\gamma}$) Kelvin branch deviates more and more from the exact Kelvin wave as $\bar{\sigma}$ decreases, approaching $\bar{\gamma}$, where the inertial motion obtains. As $\bar{\sigma}$ is further decreased there appears in the model a domain of exponential-type behaviour which is not exhibited by the two-dimensional equations; this points at a limitation of the channel model. For even smaller frequencies Kelvin-type behaviour is recovered, but a second oscillatory solution branch appears with no physical significance. Figure 7 also brings out very clearly the reflection properties of Kelvin waves. For $\bar{\sigma} > (\bar{\mu}^2 + \bar{\gamma}^2)^{\frac{1}{2}}$ a reflected Kelvin wave will be essentially of Poincaré type, since it will have a Poincaré component. For frequencies below the Sverdrup frequency, a Kelvin wave will, however, be essentially reflected as a Kelvin wave, since the reflected wave is either Kelvin-type or exponential-type.

A modification of figure 6, more appealing, better suited for a comparison with results from numerical solutions of the tidal equations, and valid for $\mu = 5$, is given in figure 8. The solid lines correspond to $\sigma^2 = \{\gamma^2\bar{\mu}^2/(4\gamma^2 + \bar{\mu}^2), \gamma^2, \gamma^2 + \bar{\mu}^2\}$ and separate the four different domains introduced above. As far as reflection of a progressing wave

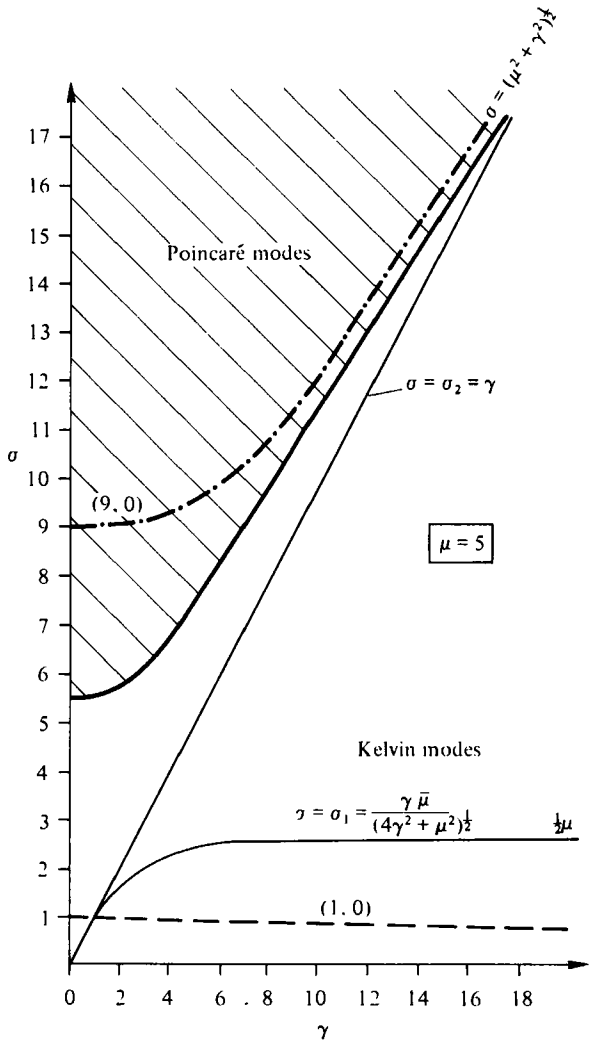

FIGURE 8. Zones for characteristic eigenmode types. In the shaded area modes have Poincaré character, in the unshaded area they are of Kelvin type. The dashed line represents the first Kelvin mode in an *enclosed* rectangle. It has one amphidromic point and is the lowest transversely antisymmetric mode; it is thus denoted by (1, 0). The dot-dashed line (9, 0) represents the first Poincaré mode arising in enclosed rectangular basins.

is concerned, only two physically significant domains need be distinguished, the Poincaré and Kelvin modes, as indicated. The domain 'Poincaré modes' is so indicated despite the possibility of Kelvin solutions (see figure 6) because incoming Kelvin-type waves are reflected by Poincaré-type waves so that the total wave exhibits Poincaré structure. Similarly, for frequencies smaller than the Sverdrup frequency of the channel model, Kelvin waves are reflected by Kelvin waves or exponential-type solutions, resulting in Kelvin-like behaviour. Figure 8 may be used to estimate whether certain oscillations arising in a basin are of Kelvin or Poincaré type. Depending on the value of γ an oscillation of given prescribed frequency may be Poincaré-type in a short and deep channel-like basin but become Kelvin-type as the channel becomes longer

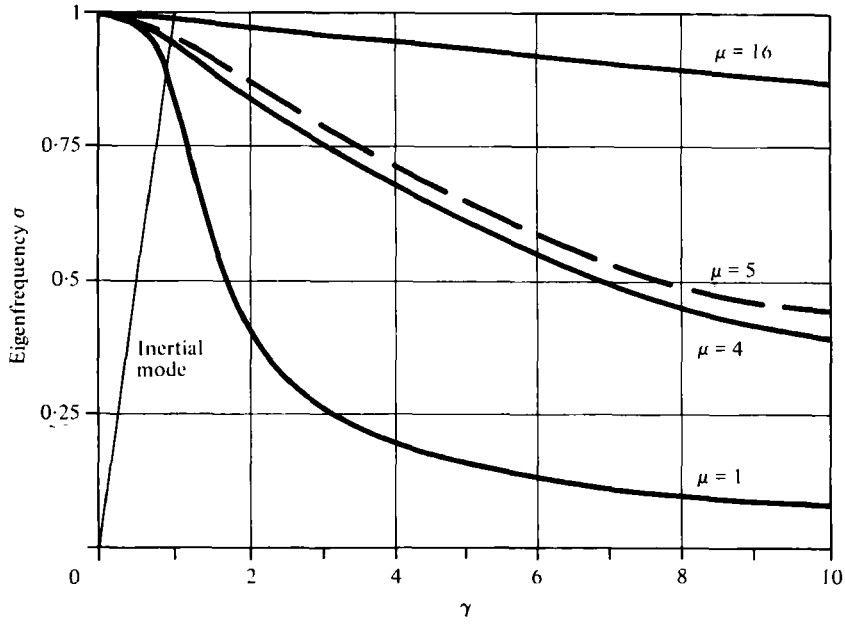

FIGURE 9. First eigenfrequency σ for a square and rectangles of length 4, 5 and 16 times their width, plotted against the rotation speed γ.

and more shallow and/or as γ increases. Such estimates may be helpful in *a priori* estimates to decide whether a certain eigenmode of a basin gives rise to both cyclonic and anticyclonic amphidromic systems.

In the remainder of this section we shall indicate how eigenfrequencies of rectangular basins of constant depth may be determined. To this end notice that, since reflections occur at two barriers, v_s, v_n, and ξ will contain terms involving $\exp(-\lambda s)$ as well as $\exp(\lambda s)$. The extra free constants occurring in the solution will then enable us to make v_s vanish at two different values of s. It is advantageous to place the origin of the co-ordinate system in the middle of the rectangle with length L and width B. The boundary-layer solutions (5.1) accounting for exponential decay away from the ends must then be replaced by

$$\left.\begin{aligned} \xi^{(0)} &= Z_0 \cosh \lambda s \cos \omega t, & \xi^{(1)} &= Z_1 \sinh \lambda s \sin \omega t, \\ v_s^{(0)} &= U_0 \sinh \lambda s \sin \omega t, & v_s^{(1)} &= U_1 \cosh \lambda s \cos \omega t, \\ v_n^{(0)} &= V_0 \sinh \lambda s \cos \omega t, & v_n^{(1)} &= V_1 \cosh \lambda s \sin \omega t, \end{aligned}\right\} \tag{5.16}$$

with the hyperbolic function selected so as to obtain the antisymmetrical elevation. For the symmetrical elevation $\cosh \lambda s$ and $\sinh \lambda s$ would have to be interchanged. Substitution of (5.16) into (4.3) yields a homogeneous linear system of equations for the amplitudes $Z_0, \ldots, V_1$. It possesses non-trivial solutions, provided that

$$\sigma^6 - \{\bar{\mu}^2 + 2(\gamma^2 - \bar{\lambda}^2)\}\sigma^4 + \{\bar{\mu}^2(\gamma^2 - \bar{\lambda}^2) + (\gamma^2 - \bar{\lambda}^2)^2\}\sigma^2 + \bar{\mu}^2\bar{\lambda}^2\gamma^2 = 0. \tag{5.17}$$

where

$$\bar{\lambda} = \lambda L/\pi. \tag{5.18}$$

For frequencies satisfying the dispersion relation (5.17) the free amplitudes in (5.16) can be determined. When this is done, one obtains

$$v_s = A_1\left\{\sinh\lambda s\sin\omega t + n\lambda\frac{\omega}{f}\frac{\lambda^2 gH+\omega^2-f^2}{\omega^2-f^2}\cosh\lambda s\cos\omega t\right\}, \tag{5.19a}$$

$$v_n = A_1\left\{\frac{\lambda^2 gH+\omega^2}{\omega f}\sinh\lambda s\cos\omega t - n\lambda\frac{\lambda^2 gH+\omega^2-f^2}{\omega^2-f^2}\cosh\lambda s\sin\omega t\right\}, \tag{5.19b}$$

$$\xi = A_1\left\{\frac{\lambda H}{\omega}\cosh\lambda s\cos\omega t + n\frac{\lambda^2 gH+\omega^2-f^2}{gf}\sinh\lambda s\sin\omega t\right\}, \tag{5.19c}$$

where A_1 is a free amplitude.

Equations (5.19*a–c*) together with (5.17) do not yet form a standing wave in an enclosed rectangle. As was the case for the reflection problem at the barrier (5.19) must be superposed with a solution that corresponds to a superposition of a forward- and backward-progressing Kelvin- or Poincaré-type wave. These solutions were constructed in § 4 and gave rise to the existence of amphidromic points. For Poincaré waves they are given in (4.15), and for Kelvin waves in (4.9) and (4.10). If we identify these solutions by the superscript 'Kelvin' and the solutions (5.19) by the superscript 'hyp' the necessary condition of no motion at the ends for Kelvin-type waves is

$$v_s^{\text{Kelvin}}(\pm\tfrac{1}{2}L, n, t) + v_s^{\text{hyp}}(\pm\tfrac{1}{2}L, n, t) = 0. \tag{5.20}$$

Substitution from (4.10) and (5.19*a*) then yields the reflection conditions at the walls

$$A_1 = -U_0\frac{\sin\frac{1}{2}\kappa L}{\sinh\frac{1}{2}\lambda L}, \tag{5.21a}$$

$$\gamma^2(\sigma^2-\gamma^2)\tanh\tfrac{1}{2}\pi\bar{\lambda} + \sigma\bar{\lambda}(\bar{\lambda}^2+\sigma^2-\gamma^2)\tan\tfrac{1}{2}\pi\sigma = 0, \tag{5.21b}$$

where U_0 is the free amplitude of the Kelvin solution (4.10). Equations (5.17) and (5.21*b*) together allow determination of the eigenfrequency of the system, and the compound solution (4.10) and (5.19) becomes

$$v_s = U_0\left\{\left[\sin\kappa s - \frac{\sin\frac{1}{2}\kappa L}{\sinh\frac{1}{2}\lambda L}\sinh\lambda s\right]\sin\omega t \right.$$
$$\left. - n\left[\frac{f}{c}\cos\kappa s + \lambda\frac{\omega}{f}\frac{\sin\frac{1}{2}\kappa L}{\sinh\frac{1}{2}\lambda L}\frac{\lambda^2c^2+\omega^2-f^2}{\omega^2-f^2}\cosh\lambda s\right]\cos\omega t\right\}, \tag{5.22a}$$

$$v_n = -U_0\frac{\sin\frac{1}{2}\kappa L}{\sinh\frac{1}{2}\lambda L}\left\{\frac{\lambda^2c^2+\omega^2}{\omega f}\sinh\lambda s\cos\omega t - n\lambda\frac{\lambda^2c^2+\omega^2-f^2}{\omega^2-f^2}\cosh\lambda s\sin\omega t\right\}, \tag{5.22b}$$

$$\xi = U_0\left(\frac{H}{g}\right)^{\frac{1}{2}}\left\{\left[\cos\kappa s - \frac{\lambda c}{\omega}\frac{\sin\frac{1}{2}\kappa L}{\sinh\frac{1}{2}\lambda L}\cos\lambda s\right]\cos\omega t \right.$$
$$\left. - n\left[\frac{f}{c}\sin\kappa s - \frac{\lambda c^2+\omega^2-f^2}{fc}\frac{\sin\frac{1}{2}\kappa L}{\sinh\frac{1}{2}\lambda L}\sinh\lambda s\right]\sin\omega t\right\}, \tag{5.22c}$$

in which $c^2 = gH$.

Numerical solutions of (5.17) and (5.21*b*) have been calculated, and a selection of results is given in figure 9. This figure displays the first eigenfrequency σ as a function of the rotational speed γ for a square and for rectangles of length 4, 5 and 16 times their width. The curve for $\mu = 5$ corresponds to the dashed line in figure 8. This mode has one amphidromic point and is the lowest-order transversely antisymmetric solution,

and is thus denoted by the symbol (1, 0). Results have also been obtained for higher-order modes; for mode (9, 0) these are shown in figure 8. It may also be recognized that for elongated rectangular basins the (1, 0) eigenfrequency is fairly insensitive to the rotational speed. The inertial mode is also shown for completeness, for it is also an eigenfrequency of the system.

It is not our intention to explore the channel approximation fully for rectangular cross-sections. One could for instance complement figure 9 with similar plots for higher frequencies, and could further treat the reflection problem by using (4.15) rather than (4.9) and (4.10). This would essentially only duplicate the exact results of Rao (1966). Rather, our intention was to search for the conditions of validity of our channel model for its use in real natural elongated basins. As far as rectangles are concerned, limitations of applicability have been found, indicating that the channel model is likely to be a valid approximation for superinertial frequencies, but may be problematic for motions at frequencies below the inertial frequency. Since superinertial frequencies are the domain of gravitational motions, and rotational modes are subinertial, we conclude that the channel approximation will predict gravitational modes reasonably. As a prelude to results presented later we mention that there arise indeed serious difficulties with the prediction of wave motion at subinertial frequencies.

6. Final remarks

The purpose of this paper was to put forward a newly developed extended channel model for the description of gravitational oscillations of a homogeneous water body on the rotating Earth. The essential features of gravitational oscillations in rectangular basins with flat bottom are well predicted. In particular, Kelvin- and Poincaré-type wave solutions in unbounded straight channels were found, and the reflection problem of Kelvin-type waves at the end of a half-open gulf was solved, as was the free oscillation in a rectangle with flat bottom using the approximate first-order linear channel equations. A further comparison of the frequency relations of the exact two-dimensional tidal operator for curved channels also indicates that, within the range of applicability of the channel model, effects of the curvature of the channel axis are negligible. The comparison of the solutions of the exact ideal operator and those of the channel model is sufficiently convincing to allow the conclusion that gravitational modes in a homogeneous water body can be accurately predicted if rotational speeds are small ($\gamma < 1$) and basins are elongated with a width-to-length ratio larger than 2. Motions at subinertial frequencies are poorly predicted, in general, but these frequencies belong to rotational rather than gravitational modes. We thus conclude, and further corroboration for this will be given in Raggio & Hutter (1982*b*) and Hutter & Raggio (1982), that the channel model is a valid one as long as gravitational modes are analysed.

In a further article (Raggio & Hutter 1982*b*) free oscillations in natural basins using the channel equations of arbitrary order are presented; it will be in that paper where additional remarks, e.g. regarding the numerical structure of the channel equations, etc. will be made.

While performing this work, G. Raggio was financially supported by the Swiss National Science Foundation through the National programme 'Basic Problems of the Swiss Water Budget', Contract No. 4.006.0.076.02, which we gratefully acknowledge.

REFERENCES

BALL, F. K. 1965 The effect of rotation on the simpler modes of motion of a liquid in an elliptic paraboloid. *J. Fluid Mech.* **22**, 529–545.

CHRYSTAL, G. 1904 Some results in the mathematical theory of seiches. *Proc. R. Soc. Edin.* **25**, 328–337.

CHRYSTAL, G. 1905 Some further results in the mathematical theory of seiches. *Proc. R. Soc. Edin.* **25**, 637–647.

CSANADY, G. T. 1972 Response of large stratified lakes to wind. *J. Phys. Oceanog.* **2**, 3–13.

DEFANT, F. 1953 Theorie der Corioliskraft. *Arch. Met. Geophys. Biokl.* (A) **6**, 218–241.

HOWARD, L. N. 1960 Lectures on fluid dynamics. In *Notes on the* 1960 *Summer Study Program in Geophysical Fluid Dynamics. Woods Hole, Mass.* (ed. E. A. Spregel), vol. 1.

HUTTER, K. & RAGGIO, G. 1982 A Chrystal-model describing gravitational barotropic motion in elongated lakes. *Arch. Met. Geophys. Biokl.* (to appear).

JOHNS, B. & HAMZAH, A. M. O. 1969 On the seiche motion in a curved lake. *Proc. Camb. Phil. Soc.* **66**, 607–615.

KELVIN, LORD 1879 On gravitational oscillations of rotating water. *Proc. R. Soc. Edin.* **10**, 92–100.

KRAUSS, W. 1973 *Methods and Results of Theoretical Oceanography, Part I, Dynamics of the Homogeneous and Quasihomogeneous Ocean.* Berlin: Gebrueder Borntraeger.

LAMB, H. 1932 *Hydrodynamics,* 6th edn. Cambridge University Press.

LAPLACE, P. S. 1829 *Mécanique Céleste* 4, no. 1. Paris: Bachelier.

LEBLOND, P. H. & MYSAK, L. A. 1978 *Waves in the Ocean.* Elsevier.

MORTIMER, C. H. 1963 Frontiers in physical limnology with particular reference to long waves in rotating basins. In *Proc. 6th Conf. Great Lakes Res., Univ. Michigan, Great Lakes Res. Div. Publ.* no. 10, pp. 9–42.

PNUELI, A. & PEKERIS, C. L. 1968 Free tidal oscillations in rotating flat basins of the form of rectangles and sectors of circles. *Proc. R. Soc. Lond.* A **263**, 149–171.

POINCARÉ, H. 1910 *Leçons de Mécanique Céleste* 3, *Théorie de Marées.* Gauthier-Villars.

RAGGIO, G. 1981 A channel model for a curved elongated homogeneous lake. Dissertation, Eidgenoessische Technische Hochschule, Zurich. *Mitteilungen* Nr 49 *der Versuchsanstalt für Wasserbau, Hydrologie und Glaziologie ETH Zürich.*

RAGGIO, G. & HUTTER, K. 1982*a* An extended channel model for the prediction of motion in elongated homogeneous lakes. Part 1. Theoretical introduction. *J. Fluid Mech.* **121**, 231–255.

RAGGIO, G. & HUTTER, K. 1982*b* An extended channel model for the prediction of motion in elongated homogeneous lakes. Part 3. Free oscillations in natural basins. *J. Fluid Mech.* **121**, 283–299.

RAO, D. B. 1966 Free gravitational oscillations in rotating rectangular basins. *J. Fluid Mech.* **25**, 523–555.

TAYLOR, G. I. 1920 Tidal oscillations in gulfs and rectangular basins. *Proc. Lond. Math. Soc.* (2) **20**, 148–181.